Improved measurement of the Triple-Gauge-Boson Couplings γWW and ZWW in e^+e^- collisions

S. Schael, R. Barate, R. Brunelière, I. de Bonis, D. Décamp, C. Goy, S. Jézéquel, J.P. Lees, F. Martin, E. Merle, et al.

EUROPEAN LABORATORY FOR NUCLEAR RESEARCH (CERN)

CERN-PH-EP/2004-065
December 8, 2004

Improved measurement of the Triple Gauge-Boson Couplings γWW and ZWW in e^+e^- collisions

The ALEPH Collaboration*

Abstract

Triple gauge-boson couplings γWW and ZWW involving single-photon, single-W and W-pair production are determined using data samples collected at LEP with the ALEPH detector at centre-of-mass energies between 183 and 209 GeV. The integrated luminosity used is $700\,\mathrm{pb}^{-1}$ for the single-photon measurement and $683\,\mathrm{pb}^{-1}$ for the W channels. Restricting the measurement to C- and P- conserving terms and applying local $\mathrm{SU(2)_L} \times \mathrm{U(1)_Y}$ gauge invariance, the measured values of the parameters g_1^Z, κ_γ and λ_γ are :

$$\begin{aligned} g_1^Z &= 1.001 \pm 0.027(\mathrm{stat.}) \pm 0.013(\mathrm{syst.}) \\ \kappa_\gamma &= 0.971 \pm 0.055(\mathrm{stat.}) \pm 0.030(\mathrm{syst.}) \\ \lambda_\gamma &= -0.012 \pm 0.027(\mathrm{stat.}) \pm 0.011(\mathrm{syst.}) \end{aligned}$$

for single-parameter fits, where the two other parameters are fixed to their Standard Model values. Results are also presented for the cases where two or all three couplings are allowed to vary.

An additional analysis using W-pair events is performed to measure the unconstrained real and imaginary parts of all 14 triple gauge-boson couplings and to perform an indirect search for a techni-ρ resonance. No deviations from the Standard Model expectations are observed and the lower limit on the techni-ρ mass is set to $600\,\mathrm{GeV}/c^2$ at 95% confidence level.

Submitted to Physics Letters B

---

*) See next pages for the list of authors

The ALEPH Collaboration

S. Schael

Physikalisches Institut das RWTH-Aachen, D-52056 Aachen, Germany

R. Barate, R. Brunelière, I. De Bonis, D. Decamp, C. Goy, S. Jézéquel, J.-P. Lees, F. Martin, E. Merle, M.-N. Minard, B. Pietrzyk, B. Trocmé

Laboratoire de Physique des Particules (LAPP), IN^{2}P^3-CNRS, F-74019 Annecy-le-Vieux Cedex, France

S. Bravo, M.P. Casado, M. Chmeissani, J.M. Crespo, E. Fernandez, M. Fernandez-Bosman, Ll. Garrido,[15] M. Martinez, A. Pacheco, H. Ruiz

Institut de Física d'Altes Energies, Universitat Autònoma de Barcelona, E-08193 Bellaterra (Barcelona), Spain[7]

A. Colaleo, D. Creanza, N. De Filippis, M. de Palma, G. Iaselli, G. Maggi, M. Maggi, S. Nuzzo, A. Ranieri, G. Raso,[24] F. Ruggieri, G. Selvaggi, L. Silvestris, P. Tempesta, A. Tricomi,[3] G. Zito

Dipartimento di Fisica, INFN Sezione di Bari, I-70126 Bari, Italy

X. Huang, J. Lin, Q. Ouyang, T. Wang, Y. Xie, R. Xu, S. Xue, J. Zhang, L. Zhang, W. Zhao

Institute of High Energy Physics, Academia Sinica, Beijing, The People's Republic of China[8]

D. Abbaneo, T. Barklow,[26] O. Buchmüller,[26] M. Cattaneo, B. Clerbaux,[23] H. Drevermann, R.W. Forty, M. Frank, F. Gianotti, J.B. Hansen, J. Harvey, D.E. Hutchcroft,[30], P. Janot, B. Jost, M. Kado,[2] P. Mato, A. Moutoussi, F. Ranjard, L. Rolandi, D. Schlatter, F. Teubert, A. Valassi, I. Videau

European Laboratory for Particle Physics (CERN), CH-1211 Geneva 23, Switzerland

F. Badaud, S. Dessagne, A. Falvard,[20] D. Fayolle, P. Gay, J. Jousset, B. Michel, S. Monteil, D. Pallin, J.M. Pascolo, P. Perret

Laboratoire de Physique Corpusculaire, Université Blaise Pascal, IN^{2}P^3-CNRS, Clermont-Ferrand, F-63177 Aubière, France

J.D. Hansen, J.R. Hansen, P.H. Hansen, A.C. Kraan, B.S. Nilsson

Niels Bohr Institute, 2100 Copenhagen, DK-Denmark[9]

A. Kyriakis, C. Markou, E. Simopoulou, A. Vayaki, K. Zachariadou

Nuclear Research Center Demokritos (NRCD), GR-15310 Attiki, Greece

A. Blondel,[12] J.-C. Brient, F. Machefert, A. Rougé, H. Videau

Laoratoire Leprince-Ringuet, Ecole Polytechnique, IN^{2}P^3-CNRS, F-91128 Palaiseau Cedex, France

V. Ciulli, E. Focardi, G. Parrini

Dipartimento di Fisica, Università di Firenze, INFN Sezione di Firenze, I-50125 Firenze, Italy

A. Antonelli, M. Antonelli, G. Bencivenni, F. Bossi, G. Capon, F. Cerutti, V. Chiarella, P. Laurelli, G. Mannocchi,[5] G.P. Murtas, L. Passalacqua

Laboratori Nazionali dell'INFN (LNF-INFN), I-00044 Frascati, Italy

J. Kennedy, J.G. Lynch, P. Negus, V. O'Shea, A.S. Thompson

Department of Physics and Astronomy, University of Glasgow, Glasgow G12 8QQ,United Kingdom[10]

S. Wasserbaech

Utah Valley State College, Orem, UT 84058, U.S.A.

R. Cavanaugh,[4] S. Dhamotharan,[21] C. Geweniger, P. Hanke, V. Hepp, E.E. Kluge, A. Putzer, H. Stenzel, K. Tittel, M. Wunsch[19]

Kirchhoff-Institut für Physik, Universität Heidelberg, D-69120 Heidelberg, Germany[16]

R. Beuselinck, W. Cameron, G. Davies, P.J. Dornan, M. Girone,[1] N. Marinelli, J. Nowell, S.A. Rutherford, J.K. Sedgbeer, J.C. Thompson,[14] R. White

Department of Physics, Imperial College, London SW7 2BZ, United Kingdom[10]

V.M. Ghete, P. Girtler, E. Kneringer, D. Kuhn, G. Rudolph

Institut für Experimentalphysik, Universität Innsbruck, A-6020 Innsbruck, Austria[18]

E. Bouhova-Thacker, C.K. Bowdery, D.P. Clarke, G. Ellis, A.J. Finch, F. Foster, G. Hughes, R.W.L. Jones, M.R. Pearson, N.A. Robertson, M. Smizanska

Department of Physics, University of Lancaster, Lancaster LA1 4YB, United Kingdom[10]

O. van der Aa, C. Delaere,[28] G.Leibenguth,[31] V. Lemaitre[29]

Institut de Physique Nucléaire, Département de Physique, Université Catholique de Louvain, 1348 Louvain-la-Neuve, Belgium

U. Blumenschein, F. Hölldorfer, K. Jakobs, F. Kayser, A.-S. Müller, B. Renk, H.-G. Sander, S. Schmeling, H. Wachsmuth, C. Zeitnitz, T. Ziegler

Institut für Physik, Universität Mainz, D-55099 Mainz, Germany[16]

A. Bonissent, P. Coyle, C. Curtil, A. Ealet, D. Fouchez, P. Payre, A. Tilquin

Centre de Physique des Particules de Marseille, Univ Méditerranée, IN^{2}P^3-CNRS, F-13288 Marseille, France

F. Ragusa

Dipartimento di Fisica, Università di Milano e INFN Sezione di Milano, I-20133 Milano, Italy.

A. David, H. Dietl,[32] G. Ganis,[27] K. Hüttmann, G. Lütjens, W. Männer[32], H.-G. Moser, R. Settles, M. Villegas, G. Wolf

Max-Planck-Institut für Physik, Werner-Heisenberg-Institut, D-80805 München, Germany[16]

J. Boucrot, O. Callot, M. Davier, L. Duflot, J.-F. Grivaz, Ph. Heusse, A. Jacholkowska,[6] L. Serin, J.-J. Veillet

Laboratoire de l'Accélérateur Linéaire, Université de Paris-Sud, IN^{2}P^3-CNRS, F-91898 Orsay Cedex, France

P. Azzurri, G. Bagliesi, T. Boccali, L. Foà, A. Giammanco, A. Giassi, F. Ligabue, A. Messineo, F. Palla, G. Sanguinetti, A. Sciabà, G. Sguazzoni, P. Spagnolo, R. Tenchini, A. Venturi, P.G. Verdini

Dipartimento di Fisica dell'Università, INFN Sezione di Pisa, e Scuola Normale Superiore, I-56010 Pisa, Italy

O. Awunor, G.A. Blair, G. Cowan, A. Garcia-Bellido, M.G. Green, T. Medcalf, A. Misiejuk, J.A. Strong, P. Teixeira-Dias

Department of Physics, Royal Holloway & Bedford New College, University of London, Egham, Surrey TW20 OEX, United Kingdom[10]

R.W. Clifft, T.R. Edgecock, P.R. Norton, I.R. Tomalin, J.J. Ward

Particle Physics Dept., Rutherford Appleton Laboratory, Chilton, Didcot, Oxon OX11 OQX, United Kingdom[10]

B. Bloch-Devaux, D. Boumediene, P. Colas, B. Fabbro, E. Lançon, M.-C. Lemaire, E. Locci, P. Perez, J. Rander, B. Tuchming, B. Vallage

CEA, DAPNIA/Service de Physique des Particules, CE-Saclay, F-91191 Gif-sur-Yvette Cedex, France[17]

A.M. Litke, G. Taylor

Institute for Particle Physics, University of California at Santa Cruz, Santa Cruz, CA 95064, USA[22]

C.N. Booth, S. Cartwright, F. Combley,[25] P.N. Hodgson, M. Lehto, L.F. Thompson

Department of Physics, University of Sheffield, Sheffield S3 7RH, United Kingdom[10]

A. Böhrer, S. Brandt, C. Grupen, J. Hess, A. Ngac, G. Prange

Fachbereich Physik, Universität Siegen, D-57068 Siegen, Germany[16]

C. Borean, G. Giannini

Dipartimento di Fisica, Università di Trieste e INFN Sezione di Trieste, I-34127 Trieste, Italy

H. He, J. Putz, J. Rothberg

Experimental Elementary Particle Physics, University of Washington, Seattle, WA 98195 U.S.A.

S.R. Armstrong, K. Berkelman, K. Cranmer, D.P.S. Ferguson, Y. Gao,[13] S. González, O.J. Hayes, H. Hu, S. Jin, J. Kile, P.A. McNamara III, J. Nielsen, Y.B. Pan, J.H. von Wimmersperg-Toeller, W. Wiedenmann, J. Wu, Sau Lan Wu, X. Wu, G. Zobernig

Department of Physics, University of Wisconsin, Madison, WI 53706, USA[11]

G. Dissertori

Institute for Particle Physics, ETH Hönggerberg, 8093 Zürich, Switzerland.

[1]Also at CERN, 1211 Geneva 23, Switzerland.

[2]Now at Fermilab, PO Box 500, MS 352, Batavia, IL 60510, USA

[3]Also at Dipartimento di Fisica di Catania and INFN Sezione di Catania, 95129 Catania, Italy.

[4]Now at University of Florida, Department of Physics, Gainesville, Florida 32611-8440, USA

[5]Also IFSI sezione di Torino, CNR, Italy.

[6]Also at Groupe d'Astroparticules de Montpellier, Université de Montpellier II, 34095, Montpellier, France.

[7]Supported by CICYT, Spain.

[8]Supported by the National Science Foundation of China.

[9]Supported by the Danish Natural Science Research Council.

[10]Supported by the UK Particle Physics and Astronomy Research Council.

[11]Supported by the US Department of Energy, grant DE-FG0295-ER40896.

[12]Now at Departement de Physique Corpusculaire, Université de Genève, 1211 Genève 4, Switzerland.

[13]Also at Department of Physics, Tsinghua University, Beijing, The People's Republic of China.

[14]Supported by the Leverhulme Trust.

[15]Permanent address: Universitat de Barcelona, 08208 Barcelona, Spain.

[16]Supported by Bundesministerium für Bildung und Forschung, Germany.

[17]Supported by the Direction des Sciences de la Matière, C.E.A.

[18]Supported by the Austrian Ministry for Science and Transport.

[19]Now at SAP AG, 69185 Walldorf, Germany

[20]Now at Groupe d' Astroparticules de Montpellier, Université de Montpellier II, 34095 Montpellier, France.

[21]Now at BNP Paribas, 60325 Frankfurt am Mainz, Germany

[22]Supported by the US Department of Energy, grant DE-FG03-92ER40689.

[23]Now at Institut Inter-universitaire des hautes Energies (IIHE), CP 230, Université Libre de Bruxelles, 1050 Bruxelles, Belgique

[24]Now at Dipartimento di Fisica e Tecnologie Relative, Università di Palermo, Palermo, Italy.

[25]Deceased.

[26]Now at SLAC, Stanford, CA 94309, U.S.A

[27]Now at CERN, 1211 Geneva 23, Switzerland

[28]Research Fellow of the Belgium FNRS

[29]Research Associate of the Belgium FNRS

[30]Now at Liverpool University, Liverpool L69 7ZE, United Kingdom

[31]Supported by the Federal Office for Scientific, Technical and Cultural Affairs through the Interuniversity Attraction Pole P5/27

[32]Now at Henryk Niewodnicznski Institute of Nuclear Physics, Polish Academy of Sciences, Cracow, Poland

1 Introduction

The existence of the triple gauge-boson couplings (TGC) in the Standard Model is a direct consequence of the $\mathrm{SU(2)_L \times U(1)_Y}$ structure of its gauge sector. The measurement of the TGCs represents a fundamental test of the non-Abelian nature of this model.

The most general Lorentz invariant parametrisation of the γWW and ZWW vertices can be described by 14 independent complex couplings [1–3], seven for each vertex: $\mathrm{g_1^V}$, $\mathrm{g_4^V}$, $\mathrm{g_5^V}$, κ_V, λ_V, $\tilde{\kappa}_\mathrm{V}$ and $\tilde{\lambda}_\mathrm{V}$, where V denotes either γ or Z. Assuming electromagnetic gauge invariance, C- and P-conservation, the set of 14 couplings can be reduced to five real parameters: $\mathrm{g_1^Z}$, κ_γ, κ_Z, λ_γ and λ_Z. Precision measurements at the Z resonance at LEP and SLC also provide bounds on the couplings [4, 5]. However, local $\mathrm{SU(2)_L \times U(1)_Y}$ gauge invariance reduces the relevance of these bounds [4] and introduces the constraints:

$$\begin{aligned} \kappa_\mathrm{Z} &= -(\kappa_\gamma - 1) \times \tan^2\theta_\mathrm{w} + \mathrm{g_1^Z} \\ \lambda_\mathrm{Z} &= \lambda_\gamma \end{aligned} \qquad (1)$$

where θ_w is the weak mixing angle. Hence, with the above constraints, only three parameters remain, with Standard Model values at tree level $\mathrm{g_1^Z}$, κ_γ=1, and λ_γ=0 [3]. The typical size of electroweak radiative corrections is $\mathcal{O}(10^{-3})$ which is an order of magnitude below the precision of the measurements presented here.

In this letter, the three couplings $\mathrm{g_1^Z}$, κ_γ and λ_γ are measured individually with the two other couplings fixed to their Standard Model values. Fits are also presented where two or all three couplings are allowed to vary simultaneously.

These measurements are performed using direct W-pair production ($\mathrm{e^+e^- \to W^+W^-}$) [6], single-W production ($\mathrm{e^+e^- \to We\nu}$) [7] and single-$\gamma$ production ($\mathrm{e^+e^- \to \nu\overline{\nu}\gamma}$) [8]. The last two channels are mainly sensitive to κ_γ and, to a lesser extent, to λ_γ. In this letter, the three final states have been analyzed using data recorded at LEP by the ALEPH detector at centre-of-mass (CM) energies between 183 and 209 GeV. These results supersede previously published measurements [9].

In addition, this letter presents results from W-pair events on unconstrained single-parameter fits to the real and imaginary parts of the six C- and P-conserving TGCs [3], and updates previous results [9] from single-parameter fits for the eight TGCs which violate either C- or P-symmetry. Of these eight TGC parameters, six are CP-violating while two, g_5^γ and g_5^Z, conserve CP. Here unconstrained means that no relationship between the TGC parameters is assumed. The only assumption is that all TGC parameters are fixed at their Standard Model values, with the exception of the fitted one.

Finally, limits are set on the mass and width of a techni-ρ resonance, defined to be the leading vector resonance in strong $\mathrm{W_L^+W_L^-}$ scattering [10–12], where $\mathrm{W_L}$ denotes a longitudinally polarized W boson. If the Higgs boson is very heavy – or absent altogether – then $\mathrm{W_L^+W_L^-}$ scattering becomes strong at high energies.

The quoted statistical errors in the following sections are defined as the 68% confidence level intervals obtained by integration of the likelihood functions, to accommodate cases with non-parabolic behaviour of the log-likelihood function.

2 The ALEPH detector and Monte Carlo generators

A detailed description of the ALEPH detector can be found in [13] and of its performance in [14]. Charged particles are detected in the central part, which consists of a precision silicon vertex detector (VDET), a cylindrical drift chamber (ITC) and a large time projection chamber (TPC), together measuring up to 31 space points along the charged particle trajectories. A 1.5 T axial magnetic field is provided by a superconducting solenoid. Charged-particle transverse momenta are reconstructed with a $1/p_{\mathrm{T}}$ resolution of $(6 \times 10^{-4} \oplus 5 \times 10^{-3}/p_{\mathrm{T}})$ $(\mathrm{GeV}/c)^{-1}$. The tracks used in the present analysis are reconstructed with at least four hits in the TPC and originate from within a cylinder of length 20 cm and radius 2 cm coaxial with the beam, centred at the nominal collision point. The charge confusion probability for a single track is negligible in the relevant momentum range.

In addition to its rôle as a tracking device, the TPC also measures the specific energy loss by ionization, $\mathrm{d}E/\mathrm{d}x$. It allows low momentum electrons to be separated from other charged particle species by more than three standard deviations up to a momentum of $8\,\mathrm{GeV}/c$.

Electrons (and photons) are also identified by the characteristic longitudinal and transverse development of the associated showers in the electromagnetic calorimeter (ECAL), a 22 radiation-length-thick sandwich of lead planes and proportional wire chambers with fine read-out segmentation. A relative energy resolution of $0.18/\sqrt{E}$ (E in GeV) is achieved for isolated electrons and photons.

Muons are identified by their characteristic penetration pattern in the hadron calorimeter (HCAL), a 1.2 m-thick iron yoke interleaved with 23 layers of streamer tubes, together with two surrounding double-layers of muon chambers. In association with the electromagnetic calorimeter, the hadron calorimeter also provides a measurement of the hadronic energy with a relative resolution of $0.85/\sqrt{E}$ (E in GeV). The specific algorithms used for lepton identification are described in [6].

The total visible energy is measured with an energy-flow reconstruction algorithm which combines all the above measurements [14]. The relative resolution on the total visible energy is $0.60/\sqrt{E}$ (E in GeV) for high multiplicity final states. In addition to the visible-energy measurement, the energy-flow reconstruction algorithm also provides a list of reconstructed objects, classified as charged particles, photons and neutral hadrons, and called *energy-flow objects* in the following. Unless otherwise specified, these energy-flow objects are the basic entities used in the present analysis.

Down to 34 mrad from the beam axis, the acceptance is closed at both ends of the experiment by the luminosity calorimeter (LCAL) [15] and a tungsten-silicon calorimeter (SICAL) [16] originally designed for the LEP1 luminosity measurement. The dead regions between the two LCAL modules at each end are covered by pairs of scintillators. The luminosity is measured with small-angle Bhabha events using the LCAL with an uncertainty less than 0.5%.

In this letter, the polar angle θ is the angle with respect to the incoming electron beam direction.

Samples of fully simulated events, reconstructed with the same program as the data, are used to compute the number of expected candidate events and particle angular distributions as a function of TGC values. The various signal and background samples provided to the W-pair and single-W analyses are listed in [6] and [7]. The samples related to the single-γ analysis are described in [8]. Signal event samples with non Standard Model TGC values were

generated by reweighting Standard Model events with weights computed by the `KoralW` [17] or `Excalibur` [18] programs.

3 W-pair production analysis

3.1 Event selection and kinematic reconstruction

For the TGC-parameter measurements using W-pair events, the relevant observables are the WW cross section and the angular distributions of the four fermions. The measurement of the WW cross section is based on events fulfilling one of the $\ell\nu q\bar{q}$, $q\bar{q}q\bar{q}$ or $\ell\nu\ell\nu$ selections, as described in [6]. The $q\bar{q}q\bar{q}$ selection is regulated by a neural network cut; in this letter the cut is fixed to 0.4, corresponding to an efficiency of 86% and a purity of 85%. The measurement of the angular distributions require the determination of the four-vector and electric charge of the four reconstructed fermions, as detailed in [9]. In order to improve the measurement of the four-vectors and to reconstruct missing neutrinos a kinematic fit, imposing energy-momentum conservation, is applied. For final states with leptons the angular analysis is restricted to events with no lepton at $|\cos\theta| > 0.95$. Only events with no reconstructed tau are included in the $\ell\nu\ell\nu$ final state. In this final state the reconstruction of two missing neutrinos requires additional constraints: both $\ell\nu$ invariant masses are fixed to the W mass value. The quadratic nature of the constraints yield a two-fold ambiguity, and the two possible solutions are folded with an equal weight. In case of a hadronic W decay, the choice between quark and anti-quark jets is not disentangled and the two possible solutions are folded. For $q\bar{q}q\bar{q}$ events, the jet pairing algorithm and W charge assignment probability (P_+) follow the procedure presented in [9]. The correct pairing is selected in about 78% of the events, out of which 79% have the right W charge assignment. These figures vary by less than 2% over the CM energy range. The numbers of selected and expected events entering in the kinematical analysis are given in Table 1.

Table 1: Numbers of selected and expected events for $\ell\nu q\bar{q}$, $q\bar{q}q\bar{q}$ and $\ell\nu\ell\nu$ channels for all CM energies. The numbers of expected signal events are also shown. The expected numbers are computed for the Standard Model values.

Channel	$\ell\nu q\bar{q}$	$q\bar{q}q\bar{q}$	$\ell\nu\ell\nu$
Data	4190	4748	372
Expected events	4153.8	4877.5	381.8
Signal events	3682.8	4141.4	353.2

For the TGC analysis, the relevant event variables are the five angles :

- θ_W, the angle between the W^- and the initial e^- in the W^+W^- rest frame; its distributions for the $\ell\nu q\bar{q}$, $q\bar{q}q\bar{q}$ and $\ell\nu\ell\nu$ decay channels are presented in Fig. 1;
- For each lepton, its polar angle θ^*_ℓ (with respect to the W flight direction) and its azimuthal angle ϕ^*_ℓ (with respect to the W-pair production plane), in the rest frame of its parent W; their distributions for the $\ell\nu q\bar{q}$ and $\ell\nu\ell\nu$ decay channels are presented in Fig. 2;

- For each quark jet, its polar and azimuthal angles, $\theta^*_{\rm jet}$ and $\phi^*{}_{\rm jet}$, in the rest frame of its parent W; their distributions for the $\ell\nu q\bar{q}$ and $q\bar{q}q\bar{q}$ decay channels are presented in Fig. 3.

For illustration, and to facilitate the combination with other LEP Collaborations [19,20], Table 2 presents the measurement of the $\cos\theta_{\rm W}$ differential cross section. This measurement is restricted to the $e\nu q\bar{q}$ and $\mu\nu q\bar{q}$ final states which have a small background contribution and a clear W charge signature. The definition of the differential cross section is based on CC03 diagrams [6] and follows the prescription of [21].

Table 2: Differential cross sections ($d\sigma^{\rm CC03}_{e/\mu\nu qq}/d\cos\theta_{\rm W}$) of W-pair production restricted to $e\nu q\bar{q}$ and $\mu\nu q\bar{q}$ final states, for different energy ranges. The expected statistical and systematic errors are given.

	Energy range			
	180-184 GeV	184-194 GeV	194-204 GeV	204-210 GeV
$\cos\theta_W$ range	$d\sigma^{\rm CC03}_{e/\mu\nu qq}/d\cos\theta_{\rm W}$ (pb)	$d\sigma^{\rm CC03}_{e/\mu\nu qq}/d\cos\theta_{\rm W}$ (pb)	$d\sigma^{\rm CC03}_{e/\mu\nu qq}/d\cos\theta_{\rm W}$ (pb)	$d\sigma^{\rm CC03}_{e/\mu\nu qq}/d\cos\theta_{\rm W}$ (pb)
$[-1.0,-0.8]$	$0.22 \pm 0.26 \pm 0.01$	$0.66 \pm 0.13 \pm 0.01$	$0.80 \pm 0.12 \pm 0.01$	$0.33 \pm 0.11 \pm 0.01$
$[-0.8,-0.6]$	$0.50 \pm 0.28 \pm 0.02$	$0.74 \pm 0.15 \pm 0.02$	$0.47 \pm 0.13 \pm 0.01$	$0.64 \pm 0.13 \pm 0.01$
$[-0.6,-0.4]$	$0.70 \pm 0.31 \pm 0.02$	$0.92 \pm 0.16 \pm 0.02$	$0.89 \pm 0.15 \pm 0.01$	$0.80 \pm 0.14 \pm 0.01$
$[-0.4,-0.2]$	$1.57 \pm 0.34 \pm 0.03$	$0.99 \pm 0.18 \pm 0.02$	$0.97 \pm 0.17 \pm 0.02$	$1.23 \pm 0.16 \pm 0.02$
$[-0.2,0.0]$	$1.29 \pm 0.38 \pm 0.02$	$1.16 \pm 0.20 \pm 0.02$	$1.32 \pm 0.19 \pm 0.02$	$1.23 \pm 0.18 \pm 0.02$
$[0.0,0.2]$	$1.95 \pm 0.42 \pm 0.02$	$2.13 \pm 0.22 \pm 0.02$	$1.89 \pm 0.21 \pm 0.02$	$1.79 \pm 0.21 \pm 0.02$
$[0.2,0.4]$	$2.45 \pm 0.46 \pm 0.04$	$2.79 \pm 0.25 \pm 0.04$	$2.23 \pm 0.24 \pm 0.03$	$2.81 \pm 0.23 \pm 0.03$
$[0.4,0.6]$	$2.23 \pm 0.52 \pm 0.05$	$3.07 \pm 0.28 \pm 0.05$	$3.58 \pm 0.28 \pm 0.05$	$2.74 \pm 0.27 \pm 0.05$
$[0.6,0.8]$	$4.54 \pm 0.60 \pm 0.05$	$3.85 \pm 0.33 \pm 0.05$	$4.43 \pm 0.34 \pm 0.05$	$4.19 \pm 0.34 \pm 0.05$
$[0.8,1.0]$	$6.09 \pm 0.71 \pm 0.07$	$5.77 \pm 0.41 \pm 0.07$	$6.38 \pm 0.43 \pm 0.08$	$8.00 \pm 0.44 \pm 0.09$

3.2 Determination of the TGCs

An optimal observable (OO) analysis [22] employing first and second order observables [23] for W-pair production in the $\ell\nu q\bar{q}$ (ℓ=e, μ or τ), $q\bar{q}q\bar{q}$ and $\ell\nu\ell\nu$ (ℓ=e, μ) final states, is performed to measure the parameters g_1^Z, κ_γ and λ_γ under the assumption of local $SU(2)_L \times U(1)_Y$ gauge invariance. With this method, the sensitive kinematical information is projected onto one dimensional distributions. Additional information from the measured total cross section is also included. A detailed description of the OO analysis is presented in [9].

In addition, a maximum likelihood (ML) analysis is employed to provide the unconstrained one-parameter limits on the real and imaginary parts of the 14 TGC parameters and to perform an indirect search for the techni-ρ.

With respect to [9], the ML analysis has been modified to accommodate the $\tau\nu q\bar{q}$, $q\bar{q}q\bar{q}$ and $\ell\nu\ell\nu$ final states. The $\tau\nu q\bar{q}$ and $q\bar{q}q\bar{q}$ final states have a strong dependency on detector response and reconstruction which is impossible in practice to parameterise using the formalism of [9]. In order to account for these effects, the log-likelihood function of the

ML analysis has been replaced for all final states by a function $f(g)$ whose derivative is given by :

$$\frac{\partial f}{\partial g} = \left(\frac{N_{\rm obs}}{N_{\rm exp}(g)} - 1 \right) \frac{\partial N_{\rm exp}(g)}{\partial g} + \sum_{i=1}^{N_{\rm obs}} \left[\frac{\partial \mu(\bar{\Omega}_i, g)/\partial g}{\mu(\bar{\Omega}_i, g)} \right] - (N_{\rm obs} - N_{\rm b})\chi_1(g) - N_{\rm b}\,\beta_1(g)$$

where g denotes a TGC parameter, $\bar{\Omega}$ are the reconstructed angles describing a W-pair event, $N_{\rm obs}$ ($N_{\rm exp}$) is the observed (expected) number of events, $N_{\rm b}$ is the expected number of background events, and $\mu(\bar{\Omega}, g)$ is the signal differential cross-section to lowest order. The function $\chi_1(g)$ corrects $\mu(\bar{\Omega}, g)$ for detector resolution, radiative corrections and all other effects as provided by the ALEPH simulation. The function $\beta_1(g)$ corrects for the background contribution. The functions $\chi_j(g)$ and $\beta_j(g)$ are defined for $j = 1, 2$ by :

$$\chi_j(g) = \int d\bar{x}\ \rho_S(\bar{x}, g) \left(\frac{\partial \mu(\bar{\Omega}(\bar{x}), g)/\partial g}{\mu(\bar{\Omega}(\bar{x}), g)} \right)^j , \qquad \beta_j(g) = \int d\bar{x}\ \rho_B(\bar{x}) \left(\frac{\partial \mu(\bar{\Omega}(\bar{x}), g)/\partial g}{\mu(\bar{\Omega}(\bar{x}), g)} \right)^j ,$$

where ρ_S (ρ_B) is the true signal (background) probability density function for events passing the selection criteria. The vector $\bar{x}$ contains the true values of all the variables required to specify ρ_S and ρ_B, and includes the four-momenta of the final-state fermions as well as the energies and angles of initial and final-state photons. In practice the functions $\chi_1(g)$ and $\beta_1(g)$ are obtained by reweighting fully simulated Monte Carlo events. The statistical error on the fitted TGC g is given by :

$$\Delta g = \left(-\frac{\partial^2 f}{\partial g^2} \right)^{-1} \sqrt{\frac{(N_{\rm obs} - N_b)^2}{N_{\rm obs}\, N_{\rm exp}^2} \left(\frac{\partial N_{\rm exp}}{\partial g} \right)^2 + (N_{\rm obs} - N_b)(\chi_2 - \chi_1^2) + N_b(\beta_2 - \beta_1^2)} \quad .$$

A function $f(g)$ whose derivative is given by the above expression for $\partial f/\partial g$ is a consistent, unbiased estimator of the TGC parameter g which includes all effects generated by simulation. The estimator $f(g)$ becomes a genuine log-likelihood estimator of the TGC g, and the statistical error reduces to the familiar $(\Delta g)^2 = (-\partial^2 f/\partial g^2)^{-1}$, in the limit that detector effects, radiative corrections, and background become negligible. This method is also used to measure the techni-ρ form factor.

3.3 Systematic uncertainties

The systematic uncertainty computation for the OO and ML analyses follows the procedure defined in [9]. Most of the sources of uncertainty having significant impact on TGC parameter measurements (luminosity determination, tracking and calorimeter simulation, hadronization, background contamination, final state interaction) are described in [6]. The other ones are listed in the following paragraphs.

Beam energy uncertainty

The CM energy uncertainty evaluated by the LEP Energy Working Group [24] is below 40 MeV. This systematic uncertainty is estimated by shifting the CM energy by ± 60 MeV when reconstructing the WW event kinematics. This shift covers also the difference between the CM energy of simulated events and the actual CM energy.

WW cross section

The theoretical precision of WW cross section estimates [25] is evaluated by comparing the predictions of `RacoonWW` [26] (using double-pole approximation [27]) and `YFSWW` [28] (based on leading-pole approximation [29]). A 0.5% systematic uncertainty is assigned.

WW angular shape

As for the W-pair cross section, the angular distributions (mainly $\cos\theta_{\mathrm{W}}$) described in Section 3.1 are affected by higher order terms. Weights associated with $\mathcal{O}(\alpha)$ corrections are computed using the `YFSWW` program and applied to the W-pair simulated events. As an example the value of λ_γ, the coupling most sensitive to the $\cos\theta_{\mathrm{W}}$ distribution, is shifted by 0.010. The uncertainty on this shift, evaluated from the precision of the theoretical calculations, is about 0.005 [30, 31]. A comparison of the `YFSWW` and `RacoonWW` predictions yields similar results [32] and is used to assign the systematic uncertainty for the description of $\mathcal{O}(\alpha)$ and missing higher order terms.

Except for the uncertainty due to the simulated statistics, which is computed for all CM energies, all other systematic uncertainties are evaluated with event samples generated at 188.6 GeV and propagated to the other CM energies. It was cross-checked that similar results are obtained with samples generated at 206.7 GeV. A summary of the systematic uncertainties for the three couplings ($\mathrm{g}_1^{\mathrm{Z}}$, κ_γ and λ_γ) and the techni-ρ form factor F_T is given in Table 3.

Table 3: Systematic uncertainties for the couplings $\mathrm{g}_1^{\mathrm{Z}}$, κ_γ, λ_γ for all CM energies and all WW channels combined. The values for the real and imaginary parts of the technipion form factor F_T (see Section 3.5) are also shown.

Source	$\mathrm{g}_1^{\mathrm{Z}}$	κ_γ	λ_γ	$Re(F_T)$	$Im(F_T)$
Luminosity determination	0.003	0.020	0.003	0.012	0.006
Beam energy	0.001	0.002	0.001	0.001	0.001
WW cross section	0.001	0.015	0.002	0.011	0.006
WW angular shape	0.006	0.012	0.005	0.002	0.004
Hadronization	0.004	0.013	0.002	0.006	0.021
Background contamination	0.001	0.010	0.002	0.003	0.002
Tracking simulation	0.002	0.012	0.002	0.005	0.008
Calorimeter simulation	0.006	0.009	0.004	0.004	0.012
Final state interaction	0.004	0.011	0.003	$<$0.001	0.006
Simulated statistics	0.002	0.010	0.002	0.009	0.016
Total	0.013	0.037	0.011	0.021	0.032

3.4 Measurements of the TGC parameters

The individual measurements of g_1^Z, κ_γ and λ_γ, for all CM energies, are given in Table 4. For each measurement, the other couplings are fixed to their Standard Model value. The results are listed for the three categories of W^+W^- decays and their combination. The corresponding log-likelihood curves are shown in Fig. 4.

Table 4: Measured values of the TGC parameters g_1^Z, κ_γ and λ_γ are given for the three categories of W^+W^- decays and their combination. Statistical and systematic errors are shown. The results at each CM energy are combined.

Channel	g_1^Z $\pm$(stat.) $\pm$ (syst.)	κ_γ $\pm$(stat.) $\pm$ (syst.)	λ_γ $\pm$(stat.) $\pm$ (syst.)
$\ell\nu q\bar{q}$	$1.004^{+0.032}_{-0.031} \pm 0.007$	$0.940^{+0.081}_{-0.071} \pm 0.030$	$-0.005^{+0.032}_{-0.031} \pm 0.009$
$q\bar{q}q\bar{q}$	$0.986^{+0.053}_{-0.049} \pm 0.041$	$1.090^{+0.162}_{-0.128} \pm 0.130$	$-0.048^{+0.056}_{-0.051} \pm 0.032$
$\ell\nu\ell\nu$	$1.044^{+0.108}_{-0.113} \pm 0.095$	$1.407^{+0.277}_{-0.282} \pm 0.230$	$0.089^{+0.106}_{-0.110} \pm 0.088$
W^+W^-	$1.001^{+0.027}_{-0.026} \pm 0.013$	$0.979^{+0.072}_{-0.064} \pm 0.037$	$-0.012^{+0.027}_{-0.026} \pm 0.011$

Results from one-parameter fits of the unconstrained real and imaginary parts of the six TGCs that are both C- and P-conserving are given in Table 5.

Table 5: Measured coupling parameters for the unconstrained real and imaginary parts of the TGC parameters that are both C- and P- conserving. Also shown are the results for the real and imaginary parts of the technipion form factor F_T (see Section 3.5). The corresponding 95% confidence intervals are listed in the last column. The Standard Model value for the real part is displayed in the first column while all imaginary components are equal to zero.

Parameter	Real			Imaginary	
	S.M. value	Fit result $\pm$(stat. $\oplus$ syst.)	95% confidence level interval	Fit result $\pm$(stat. $\oplus$ syst.)	95% confidence level interval
κ_γ	1	1.071 ± 0.061	[0.956, 1.193]	0.070 ± 0.087	[-0.103, 0.236]
λ_γ	0	0.096 ± 0.066	[-0.028, 0.229]	0.002 ± 0.071	[-0.137, 0.142]
g_1^γ	1	1.123 ± 0.082	[0.967, 1.289]	0.030 ± 0.104	[-0.173, 0.231]
κ_Z	1	1.065 ± 0.060	[0.949, 1.182]	0.053 ± 0.058	[-0.062, 0.165]
λ_Z	0	0.019 ± 0.054	[-0.086, 0.125]	0.003 ± 0.045	[-0.086, 0.092]
g_1^Z	1	1.066 ± 0.076	[0.920, 1.214]	0.023 ± 0.068	[-0.110, 0.156]
F_T	1	0.966 ± 0.049	[0.868, 1.061]	-0.147 ± 0.096	[-0.332, 0.044]

The results from the one-parameter fits of the real and imaginary parts of the eight TGCs that violate either C- or P-symmetry are shown in Table 6.

Table 6: Measured coupling parameters for the unconstrained real and imaginary parts of TGCs that violate either C- or P-conservation. The corresponding 95% confidence intervals are listed in the last column. The Standard Model values for real and imaginary parts are equal to zero.

Parameter	Real		Imaginary	
	Fit result $\pm$(stat. $\oplus$ syst.)	95% confidence level interval	Fit result $\pm$(stat. $\oplus$ syst.)	95% confidence level interval
$\tilde{\kappa}_\gamma$	-0.088 ± 0.114	[-0.307, 0.138]	-0.036 ± 0.061	[-0.156, 0.084]
$\tilde{\lambda}_\gamma$	0.059 ± 0.087	[-0.112, 0.223]	0.041 ± 0.048	[-0.053, 0.134]
$\tilde{\kappa}_Z$	-0.089 ± 0.063	[-0.209, 0.037]	-0.034 ± 0.044	[-0.121, 0.053]
$\tilde{\lambda}_Z$	0.064 ± 0.048	[-0.032, 0.154]	0.032 ± 0.035	[-0.038, 0.101]
g_4^γ	0.058 ± 0.161	[-0.261, 0.369]	0.051 ± 0.143	[-0.227, 0.330]
g_5^γ	-0.043 ± 0.209	[-0.456, 0.363]	-0.169 ± 0.245	[-0.641, 0.312]
g_4^Z	0.134 ± 0.107	[-0.080, 0.341]	0.102 ± 0.103	[-0.100, 0.302]
g_5^Z	-0.064 ± 0.130	[-0.317, 0.190]	-0.074 ± 0.153	[-0.371, 0.225]

3.5 The technipion form factor F_T and the techni-ρ mass

In analogy with $e^+e^- \to \pi^+\pi^-$ and the ρ resonance, the effect of a techni-ρ resonance on $e^+e^- \to W_L^+W_L^-$ can be described by the complex technipion form factor F_T [33] :

$$F_T = \frac{M_\rho^2 - i\Gamma_\rho M_\rho}{M_\rho^2 - s - i\Gamma_\rho M_\rho} \quad ,$$

where M_ρ and Γ_ρ are the mass and width of the techni-ρ, respectively. Limits are placed on M_ρ and Γ_ρ by measuring the real and imaginary parts of F_T.

The results for the one-parameter fits of the real and imaginary parts of the technipion form factor F_T are shown in Table 5. The real/imaginary part of F_T is fixed at its Standard Model value when fitting its imaginary/real part.

In order to convert the measurement of F_T into limits on the techni-ρ mass and width, $M_\rho > \sqrt{s}$ is assumed. Under this assumption the true values of $\Delta Re(F_T) = Re(F_T) - 1$ and $Im(F_T)$ are always positive, and the one-parameter fit of $Re(F_T)$ is independent of the true value of $Im(F_T)$ and vice versa. The independence of the one-parameter fits implies that the central values and errors for $Re(F_T)$ and $Im(F_T)$ can be used to form a binormal distribution of $Re(F_T)$ and $Im(F_T)$. The 95% confidence limit (CL) contour for this binormal distribution is shown in Fig. 5a. The solid shaded area in Fig. 5a indicates the allowed 95% CL region for the true value of F_T calculated using the method of Feldman and Cousins [34]. The solid shaded region of Fig. 5a is mapped onto the $(M_\rho, \Gamma_\rho/M_\rho)$ plane in Fig. 5b.

The solid shaded area in Fig. 5b is the 95% CL allowed region, and implies $M_\rho > 696\,\mathrm{GeV}$ at 95% CL assuming $\Gamma_\rho/M_\rho < 0.5$. The techni-ρ mass limit is reduced to $M_\rho > 600\,\mathrm{GeV}$ at 95% CL if values for the width as large as $\Gamma_\rho/M_\rho = 1.0$ are allowed.

4 Single-W production analysis

Assuming $\mathrm{SU(2)_L \times U(1)_Y}$ gauge invariance, single-W event production is sensitive to κ_γ and λ_γ. The TGC measurement is derived from the total rate of single-W events presented in [7]. The total systematic uncertainties are ± 0.061 for κ_γ and ± 0.192 for λ_γ, dominated by the uncertainty on the precision on theoretical cross-section computation (5%) [25].

The measured values of the coupling parameters are :

$$\begin{aligned} \kappa_\gamma &= 0.925^{+\,0.094}_{-\,0.105}(\mathrm{stat.}) \pm 0.061(\mathrm{syst.}) \\ \lambda_\gamma &= -0.168^{+\,0.424}_{-\,0.269}(\mathrm{stat.}) \pm 0.192(\mathrm{syst.}) \quad , \end{aligned}$$

each measurement being performed with the other coupling set to its Standard Model value. The corresponding log-likelihood functions are presented in Fig. 6.

5 Single-photon production analysis

Assuming $\mathrm{SU(2)_L \times U(1)_Y}$ gauge invariance, independent constrains on κ_γ and λ_γ are obtained in the single photon production. The single-photon event selection, described in [35], has been applied to all CM energies, corresponding to an integrated luminosity of 700.4 pb^{-1}. A total of 1072 events is found in the data sample, while, for the Standard Model TGC values, 1142 signal events are expected. For the TGC measurement, the computation of the associated weights are described in [36].

The discriminating variables used to perform a likelihood fit to the data are the expected number of events, the scaled photon energy $x_\mathrm{E} = E_\gamma/E_\mathrm{beam}$ and the cosine of the polar angle of the photon $|\cos\theta_\gamma|$.

The systematic uncertainties are estimated following the procedure described in [9]; the most important contributions are photon energy calibration and theoretical model uncertainties. The total systematic uncertainty amounts to ± 0.16 on κ_γ and ± 0.18 on λ_γ. The TGC measured values are :

$$\begin{aligned} \kappa_\gamma &= 0.95^{+\,0.30}_{-\,0.25}(\mathrm{stat.}) \pm 0.16(\mathrm{syst.}) \\ \lambda_\gamma &= 0.10 \pm 0.35(\mathrm{stat.}) \pm 0.18(\mathrm{syst.}) \quad , \end{aligned}$$

each measurement being performed with the other coupling set to its Standard Model value. The corresponding log-likelihood functions are presented in Fig. 6.

6 Combined measurements of constrained TGC parameters

Measurements of $\mathrm{g_1^Z}$, κ_γ and λ_γ assuming $\mathrm{SU(2)_L \times U(1)_Y}$ gauge invariance, with W-pair, single-W and single-γ events are combined by adding the log-likelihoods. Single-parameter fit results are listed in Table 7 and corresponding log-likelihood curves are shown in Fig. 6. The associated 95% confidence level intervals are :

$$
\begin{aligned}
0.946 < \quad & g_1^Z & < \quad 1.061 \\
0.857 < \quad & \kappa_\gamma & < \quad 1.010 \\
-0.066 < \quad & \lambda_\gamma & < \quad 0.047.
\end{aligned}
$$

To study the full correlation between parameters, two- and three-parameter fits, where two or all three couplings are allowed to vary, were also studied. For the three parameter fit, results and errors (including the systematic uncertainties) computed as the values for which the log-likelihood changes by 0.5 units from its minimum value, are summarised in Table 8. In the same table, the associated correlation matrix evaluated at the local minimum is also given. Projections on two-dimensional planes of the three-dimensional envelope of the 95% confidence level volume, representing the integration of the confidence over the corresponding third coupling, are shown in Fig. 7. The 95% confidence limits of the 2-parameter fits of the three pairs of couplings (g_1^Z, κ_γ), (g_1^Z, λ_γ) and (λ_γ, κ_γ) are shown as dashed lines.

Table 7: Measured values of the TGC parameters g_1^Z, κ_γ and λ_γ. The statistical and systematic errors are shown.

Channel	g_1^Z $\pm$(stat.) $\pm$ (syst.)	κ_γ $\pm$(stat.) $\pm$ (syst.)	λ_γ $\pm$(stat.) $\pm$ (syst.)
W^+W^-	$1.001^{+0.027}_{-0.026} \pm 0.013$	$0.979^{+0.072}_{-0.064} \pm 0.037$	$-0.012^{+0.027}_{-0.026} \pm 0.011$
Single-W	-	$0.925^{+0.094}_{-0.105} \pm 0.061$	$-0.168^{+0.424}_{-0.269} \pm 0.192$
Single-γ	-	$0.950^{+0.300}_{-0.250} \pm 0.160$	$0.100 \pm 0.350 \pm 0.180$
Combined	$1.001^{+0.027}_{-0.026} \pm 0.013$	$0.971^{+0.057}_{-0.054} \pm 0.030$	$-0.012^{+0.027}_{-0.026} \pm 0.011$

Table 8: Result of a three-parameter fit for g_1^Z, κ_γ and λ_γ using the combined information from W-pair, single-γ and single-W productions for all CM energies. The combined statistical and systematic errors are defined as the values for which the log-likelihood changes by 0.5 units from its maximum value. The corresponding correlations are given in the last column.

Coupling	Fit result $\pm$(stat.) $\pm$ (syst.)	Correlation g_1^Z	κ_γ	λ_γ
g_1^Z	$1.042^{+0.036}_{-0.048} \pm 0.013$	1.0	-0.17	-0.62
κ_γ	$0.951^{+0.060}_{-0.047} \pm 0.030$		1.0	-0.15
λ_γ	$-0.040^{+0.036}_{-0.036} \pm 0.011$			1.0

7 Summary and conclusion

The real and imaginary parts of the 14 unconstrained triple gauge-boson couplings parameters are measured separately using W-pair events collected by the ALEPH detector at centre-of-mass energies between 183 and 209 GeV. No deviation from the Standard Model expectation is observed.

The measurement of the three constrained triple gauge-boson couplings g_1^Z, κ_γ and λ_γ have also been performed using W-pair, single-W and single-γ events. The results for single-parameter fits are :

$$\begin{aligned} g_1^Z &= 1.001 \pm 0.027(\text{stat.}) \pm 0.013(\text{syst.}) \\ \kappa_\gamma &= 0.971 \pm 0.055(\text{stat.}) \pm 0.030(\text{syst.}) \\ \lambda_\gamma &= -0.012 \pm 0.027(\text{stat.}) \pm 0.011(\text{syst.}) \quad , \end{aligned}$$

where the two other parameters are fixed to their Standard Model values. Multi-parameter fits of two or the three couplings have also been performed. The measured values are in agreement with the Standard Model expectation.

Finally, W-pair events are analysed to probe for the existence of a techni-ρ resonance through $W_L^+W_L^-$ production. No deviation from the Standard Model prediction is observed and the 95% confidence level intervals on the associated technipion form factor are:

$$\begin{aligned} 0.868 < \quad & Re(F_T) \quad < 1.061 \\ -0.332 < \quad & Im(F_T) \quad < 0.044 \quad . \end{aligned}$$

This corresponds to a lower limit on the techni-ρ mass of $600\,\text{GeV}/c^2$ at 95% confidence level, assuming that its width is less than its mass.

All measurements are statistically limited. Similar analyses have been performed by other experiments at LEP [37–40] and at the Tevatron [41].

Acknowledgements

It is a pleasure to congratulate our colleagues from the CERN accelerator divisions for the very successful operation of LEP at high energies. We are indebted to the engineers and technicians in all our institutions for their contributions to the excellent performance of ALEPH. Those of us from non-member countries thank CERN for its hospitality.

References

[1] K. Hagiwara, R. D. Peccei, D. Zeppenfeld and K. Hikasa, Nucl. Phys. **B282** (1987) 253.

[2] M. Bilenky, J.L. Kneur, F.M. Renard and D. Schildknecht, Nucl. Phys. **B409** (1993) 22.

[3] G. Gounaris, J.-L. Kneur and D. Zeppenfeld, from *Physics at LEP2*, CERN 96-01 p. 525, editors G. Altarelli, T. Sjöstrand and F. Zwirner.

[4] A. De Rújula, M. B. Gavela, P. Hernandez and E. Massó, Nucl. Phys. **B384** (1992) 3.

[5] J. Ellison and J. Wudka, Ann. Rev. Nucl. Part. Sci. **48** (1998) 33.

[6] The ALEPH collaboration, *Measurement of W-pair production in e^+e^- collisions at centre-of-mass energies from 183 to 209 GeV*, CERN-EP-PH-2004-012, accepted for publication in European Physical Journal C.

[7] The ALEPH collaboration, *Single vector boson production in e^+e^- collisions at centre-of-mass energies from 183 to 209 GeV*, CERN-EP-PH-2004-034, accepted for publication in Physics Letters B.

[8] The ALEPH collaboration, *Single- and multi-photon production in e^+e^- collisions at $\sqrt{s}$ up to 209 GeV*, Eur. Phys. J. **C28** (2003) 1.

[9] The ALEPH Collaboration, *Measurement of Triple Gauge-Boson Couplings at LEP energies up to 189 GeV*, Eur. Phys. J. **C21** (2001) 423.

[10] S. Weinberg, Phys. Rev. D **13** (1976) 974.

[11] L. Susskind, Phys. Rev. D **20** (1979) 2619.

[12] C. T. Hill and E. H. Simmons, Phys. Rept. **381** (2003) 235 [Erratum-ibid. **390** (2004) 553]

[13] The ALEPH Collaboration, *ALEPH: a detector electron-positron annihilations at LEP*, Nucl. Instrum. and Methods **A294** (1990) 121.

[14] The ALEPH Collaboration, *Performance of the ALEPH detector at LEP*, Nucl. Instrum. and Methods **A360** (1995) 481.

[15] The ALEPH Collaboration, *Measurement of the absolute luminosity with the ALEPH detector*, Zeit. Phys. **C53** (1992) 375.

[16] D. Bederede *et al.*, *SICAL - a high precision silicon-tungsten calorimeter for ALEPH*, Nucl. Instrum. and Methods **A365** (1995) 117.

[17] S. Jadach *et al.*, Comp. Phys. Commun. **140** (2001) 475.

[18] F.A. Berends, R. Kleiss and R. Pittau, Comp. Phys. Commun. **85** (1995) 437.

[19] The DELPHI Collaboration, *Measurement of the W-pair Production Cross-section and W Branching Ratios in e^+e^- Collisions at $\sqrt{s}$ = 161-209 GeV*, Eur. Phys. J. **C34** (2004) 127.

[20] The L3 Collaboration, *Measurement of the Cross Section of W-boson pair production at LEP*, Phys. Lett. **B600** (2004) 22.

[21] *A combination of Preliminary Electroweak Measurements and Constraints on the Standard Model*, hep-ex/0412015.

[22] M. Diehl and O. Nachtmann, Zeit. Phys. **C62** (1994) 397.

[23] D.K. Fanourakis, D. Fassouliotis and S.E. Tzamarias, Nucl. Instrum. and Methods **A412** (1998) 465; Nucl. Instrum. and Methods **A414** (1998) 399.

[24] R. Assman *et al.*, *Calibration of the centre-of-mass energies at LEP2 for a precise measurement of the W boson mass*, CERN-PH-EP-2004-032, CERN-AB-2004-030 OP.

[25] *Reports of the Working Groups on Precision Calculations for LEP2 physics*, edited by S. Jadach, G. Passarino and R. Pittau (CERN 2000-009, Geneva, 2000).

[26] A. Denner, S. Dittmaier, M. Roth and D. Wackeroth, Nucl. Phys. **B560** (1999) 33; Phys. Lett. **B475** (2000) 127; Eur. Phys. J. direct **C4** (2000) 1.

[27] A. Denner, S. Dittmaier, M. Roth and D. Wackeroth, Nucl. Phys. **B587** (2000) 67.

[28] S. Jadach *et al.*, Comp. Phys. Commun. **140** (2001) 432.

[29] R. Stuart, Nucl. Phys. **B498** (1997) 28.

[30] R. Brunelière, *Mesure des couplages à trois bosons dans l'expérience ALEPH au LEP*, Thèse de Doctorat de l'Université de Savoie (2003), LAPP-T-2003/02 and CERN-THESIS-2003-018.

[31] R. Brunelière *et al.*, Phys. Lett. **B533** (2002) 75.

[32] M. Dierckxsens, *Measurement of Triple Gauge Boson Couplings in e^+e^- Collisions at LEP*, Ph. D. thesis, University of Nijmegen, 2004.

[33] T. L. Barklow *et al.*, "Strong coupling electroweak symmetry breaking," in *Proc. of DPF/DPB Summer Study on New Directions for High Energy Physics (Snowmass 1996)*, Snowmass, Colorado, eConf **C960625** (1996) STC118.

[34] G. J. Feldman and R. D. Cousins, Phys. Rev. D **57** (1998) 3873.

[35] The ALEPH Collaboration, *Measurement of triple gauge $WW\gamma$ couplings at LEP2 using photonic events*, Phys. Lett. **B445** (1998) 239.

[36] A. Jacholkowska, J. Kalinowski and Z. Wąs, Comp. Phys. Commun. **124** (2000) 238; A. Jacholkowska, J. Kalinowski and Z. Wąs, Eur. Phys. J. **C6** (1999) 485.

[37] The L3 Collaboration, *Measurement of Triple-Gauge-Boson Couplings of the W boson at LEP*, Phys. Lett. **B586** (2004) 151.

[38] The L3 Collaboration, *Production of Single W Bosons at LEP and Measurement of $WW\gamma$ Gauge Coupling Parameters*, Phys. Lett. **B547** (2002) 151.

[39] The DELPHI Collaboration, *Measurement of Trilinear Gauge Boson Couplings WWV, (V≡Z,γ) in e^+e^- Collisions at 189 GeV*, Phys. Lett. **B502** (2001) 9.

[40] The OPAL Collaboration, *Measurement of charged current triple gauge boson couplings using W pairs at LEP*, Eur. Phys. J. **C33** (2004) 463.

[41] The DØ Collaboration, *Limits on anomalous $WW\gamma$ and WWZ couplings from $WW/WZ \to e\nu jj$ production*, Phys. Rev. **D62** (2000) 052005.

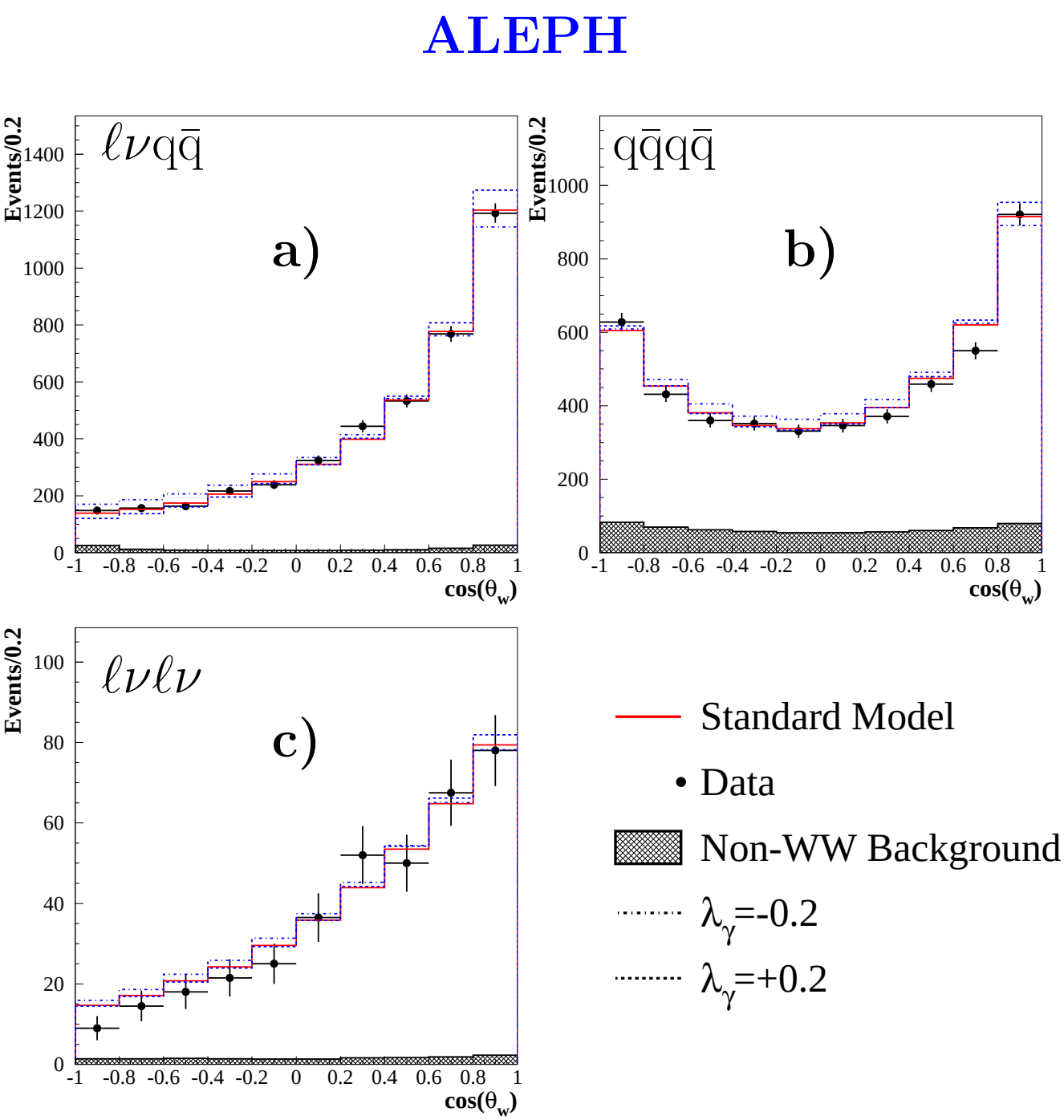

Figure 1: Distributions of the cosine of the W^- production angle $\cos\theta_W$ for a) $\ell\nu q\bar{q}$, b) $q\bar{q}q\bar{q}$ and c) $\ell\nu\ell\nu$ channels. For $q\bar{q}q\bar{q}$ events, each event enters with two solutions in the distributions with the weights P_+ and $1-P_+$, where P_+ is the probability for a di-jet pair to be a W^+. For $\ell\nu\ell\nu$ events, each event enters with two solutions with a weight of 0.5. Data are represented by solid dots. The solid line shows the Standard Model prediction while dashed and dashed-dotted histograms display the effect of $\lambda_\gamma = +0.2$ and $\lambda_\gamma = -0.2$. The background contribution is represented by the hatched area.

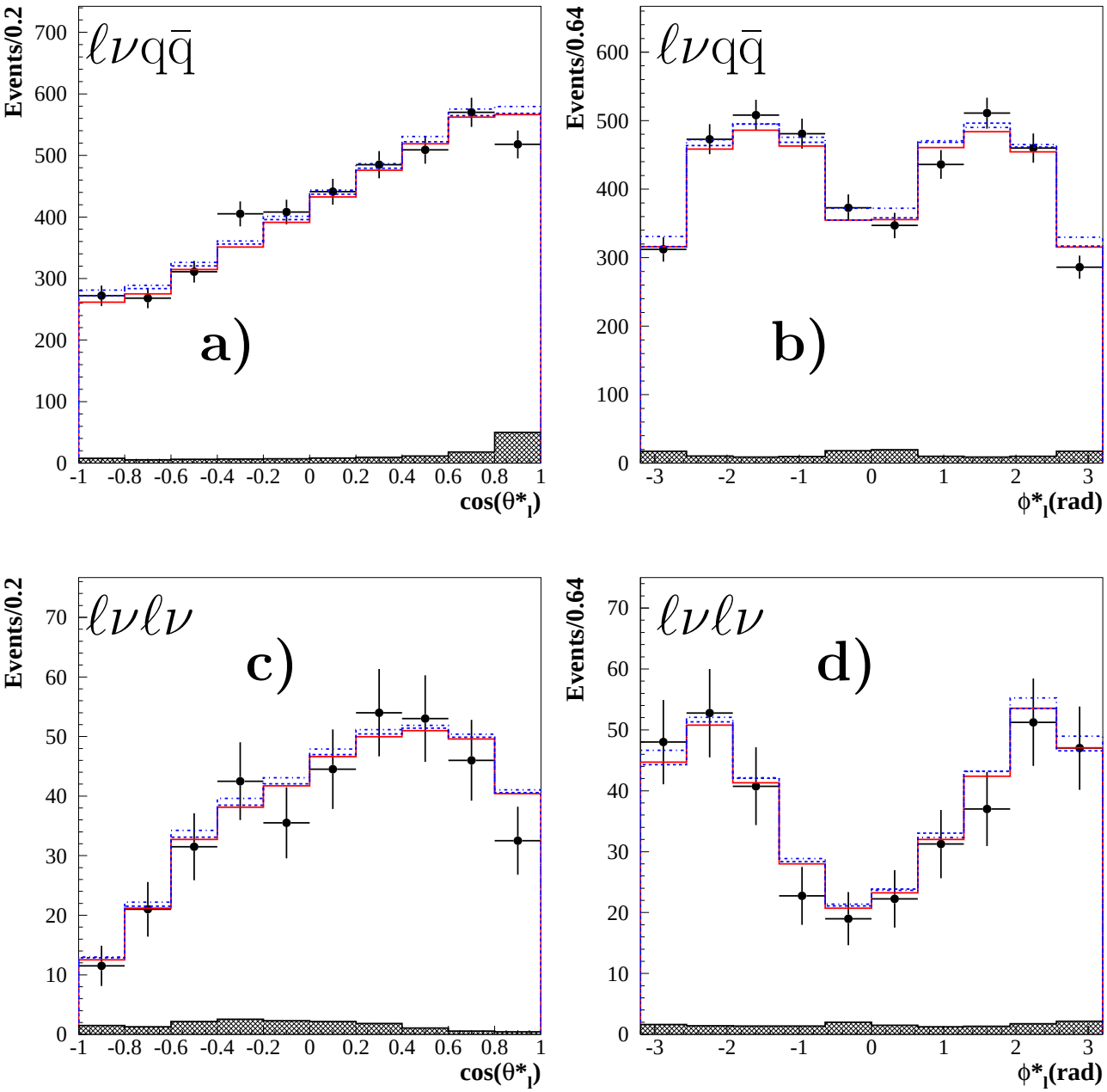

Figure 2: Distributions of the lepton polar and azimuthal angles, $\cos\theta^*_\ell$ and ϕ^*_ℓ, in the rest frame of its parent W for $\ell\nu q\bar{q}$ a) and b) and for $\ell\nu\ell\nu$ c) and d). For $\ell\nu\ell\nu$ events, each lepton for each of the two ambiguous solutions enters with a weight of 0.25 . Data are represented by solid dots. The solid line shows the Standard Model prediction while dashed and dashed-dotted histograms display the effect of $\lambda_\gamma = +0.2$ and $\lambda_\gamma = -0.2$. The background contribution is represented by the hatched area.

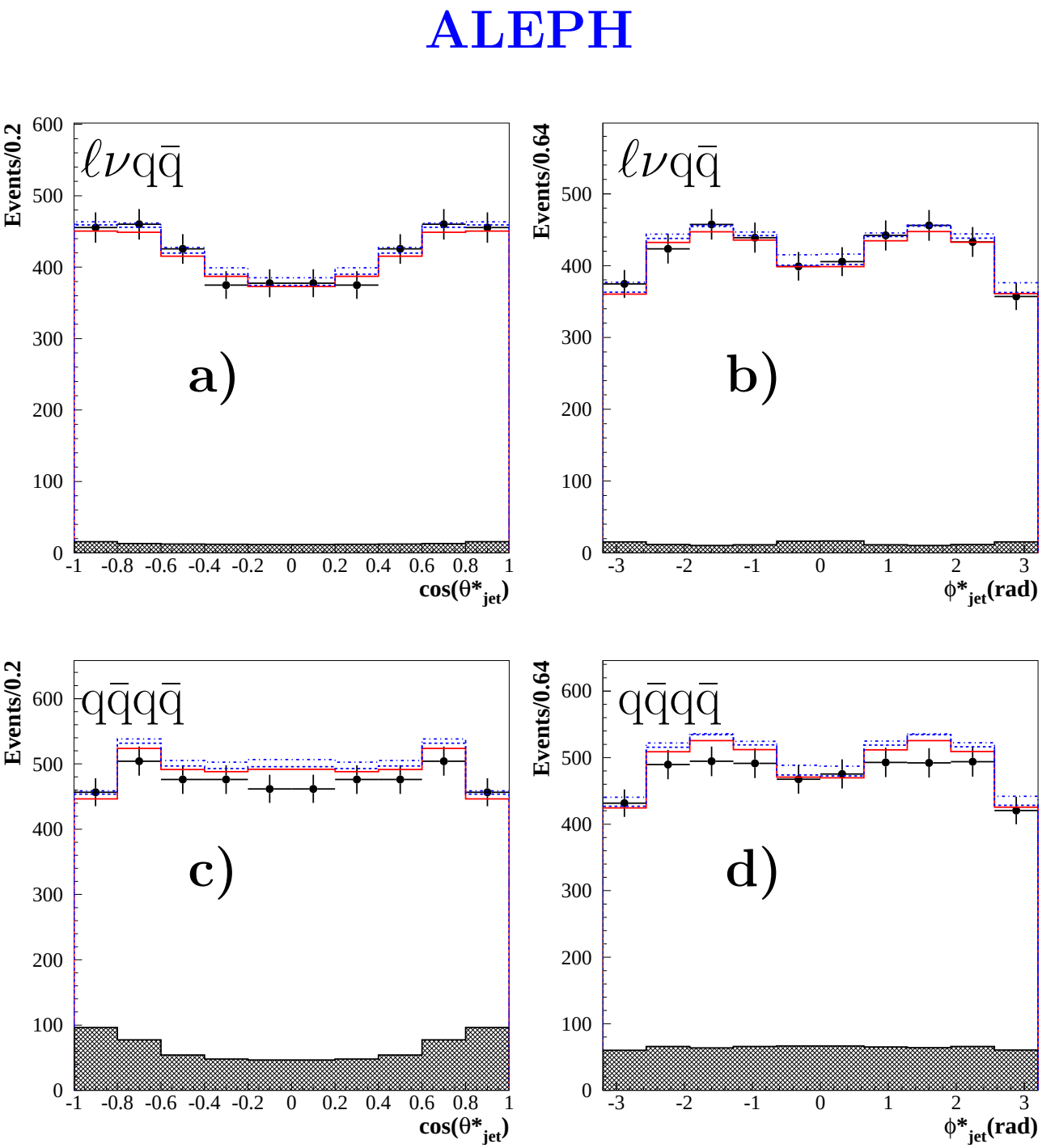

Figure 3: Distributions of the polar and azimuthal angles, $\cos\theta^*_{\rm jet}$ and ϕ^*_{jet}, of the jets in the rest frame of its parent W for $\ell\nu q\bar{q}$ a) and b) and for $q\bar{q}q\bar{q}$ c) and d). Within a W boson, the choice between quark and anti-quark jets is ambiguous. The two (four) possible choices are filled in the histogram with a weight of 0.5 for the $\ell\nu q\bar{q}$ channel (0.25 for the $q\bar{q}q\bar{q}$ channel). Data are represented by solid dots. The solid line shows the Standard Model prediction while dashed and dashed-dotted histograms display the effect of $\lambda_\gamma = +0.2$ and $\lambda_\gamma = -0.2$. The background contribution is represented by the hatched area.

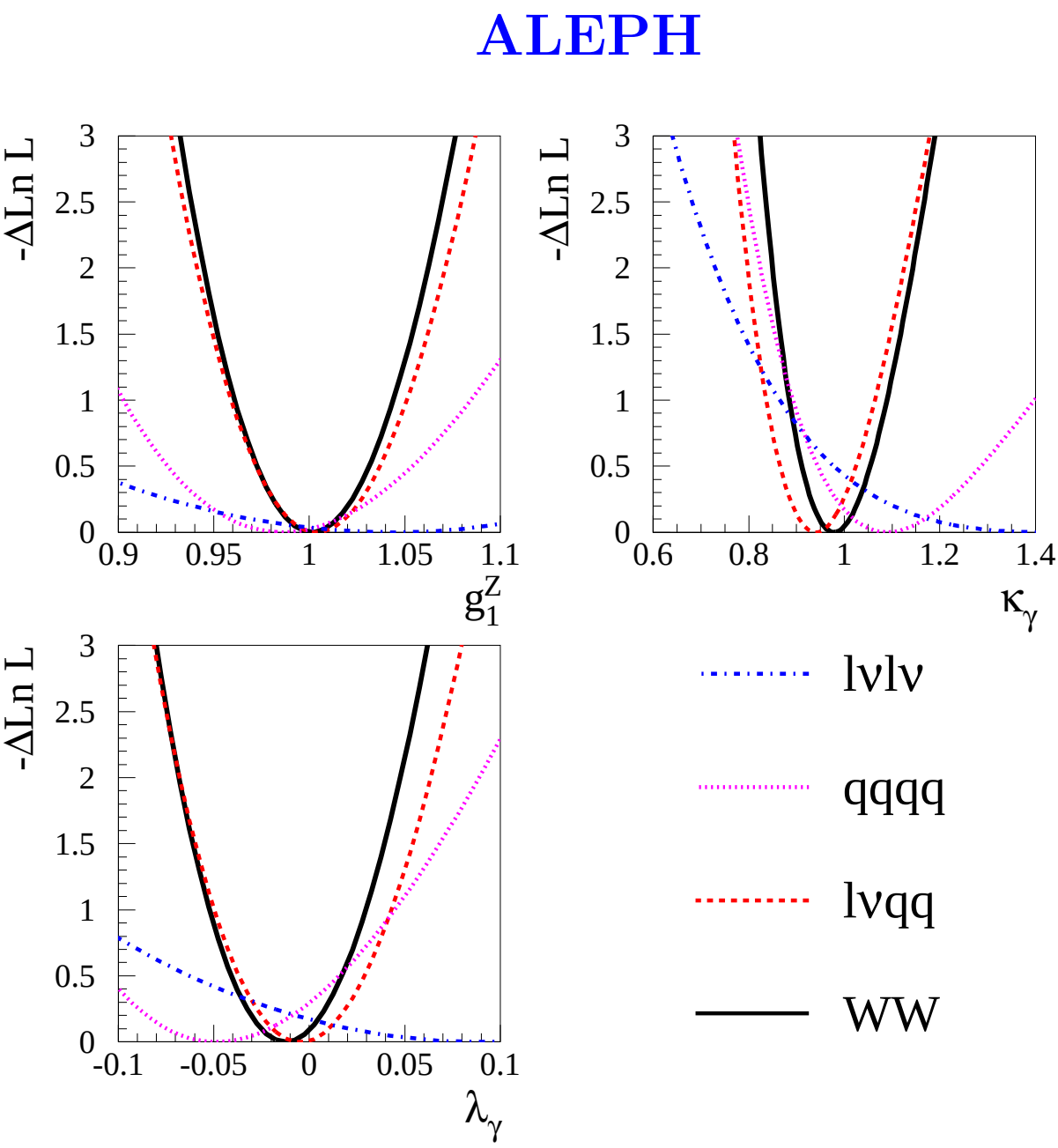

Figure 4: The negative log-likelihood curves of the single-parameter fits in the $\ell\nu q\bar{q}$ (dashed line), $q\bar{q}q\bar{q}$ (dotted line) and $\ell\nu\ell\nu$ (dashed-dotted line) channels for the three couplings g_1^Z, κ_γ and λ_γ, measured using W-pair events at all CM energies. The combined result corresponds to the solid curve. The curve for each coupling is obtained fixing the other couplings to their Standard Model values assuming $SU(2)_L \times U(1)_Y$ gauge invariance. The systematic uncertainties are included.

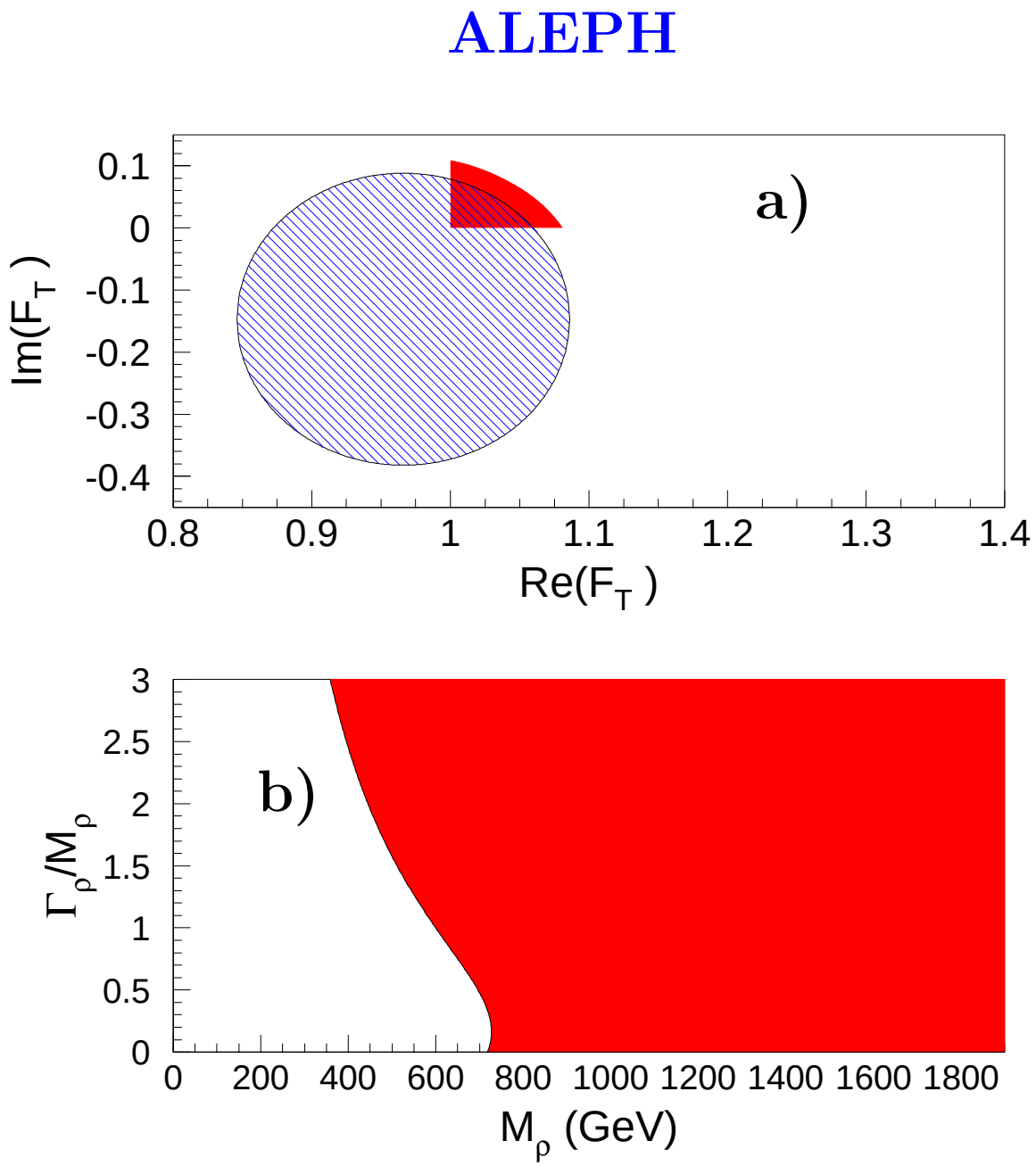

Figure 5: In (a) the hatched 95% CL ellipse for the measured real and imaginary parts of the technipion form factor F_T is shown centered on $(Re(F_T), Im(F_T)) = (0.97, -0.15)$. The solid shaded area indicates the allowed 95% CL region for the true value of F_T calculated using the Feldman-Cousins method. Points within the solid shaded area of (a) are mapped onto the $(M_\rho, \Gamma_\rho/M_\rho)$ plane in (b). The white region in (b) is thus excluded at 95% CL.

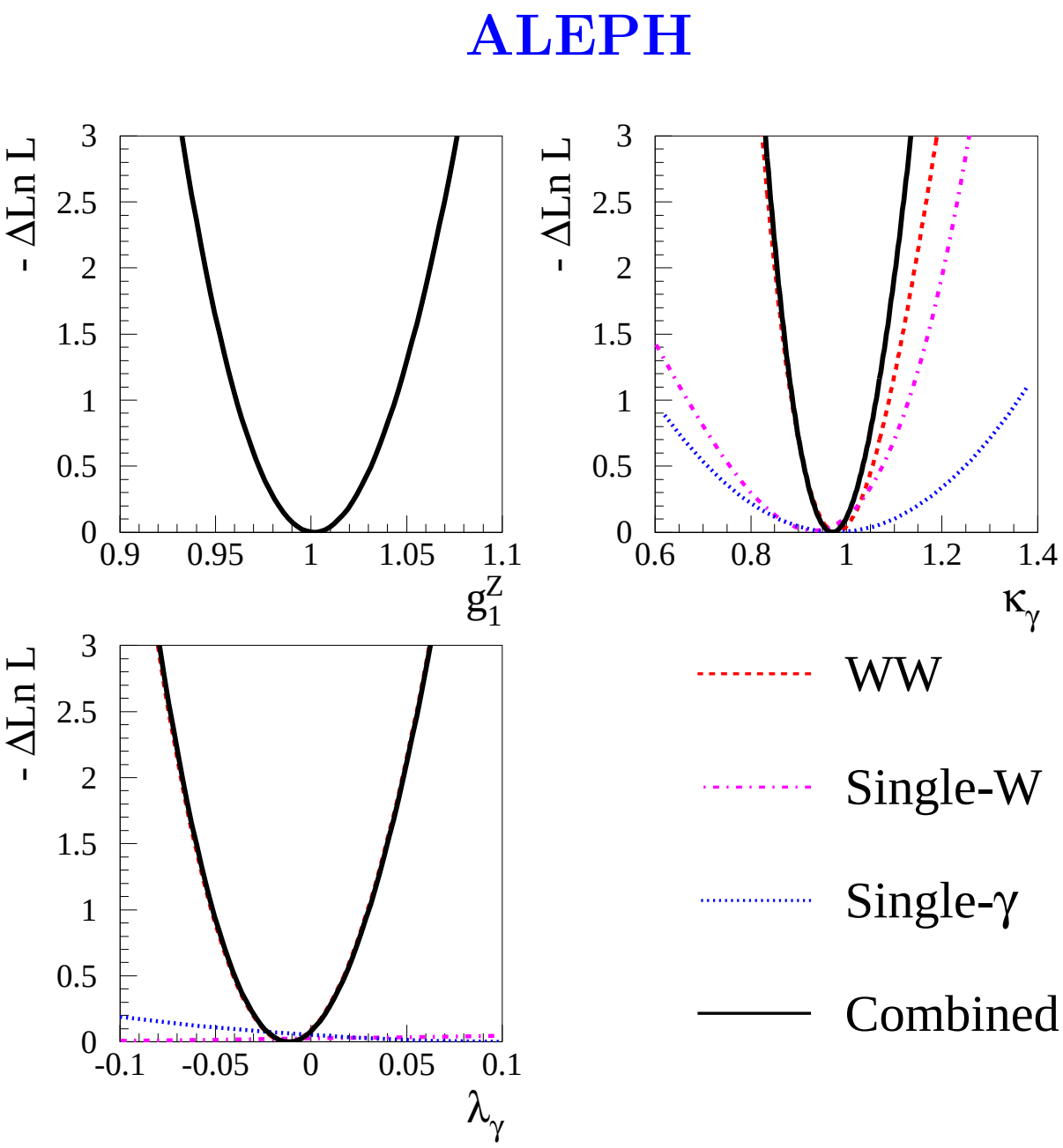

Figure 6: The negative log-likelihood curves of the single-parameter fits using W-pair (dashed line), single-W (dashed-dotted line) and single-γ (dotted line) events for the three couplings g_1^Z, κ_γ and λ_γ including all CM energies. The combined result is shown as the solid curve. The curve for each coupling parameter is obtained fixing the other couplings to their Standard Model values assuming $SU(2)_L \times U(1)_Y$ gauge invariance. The systematic uncertainties are included.

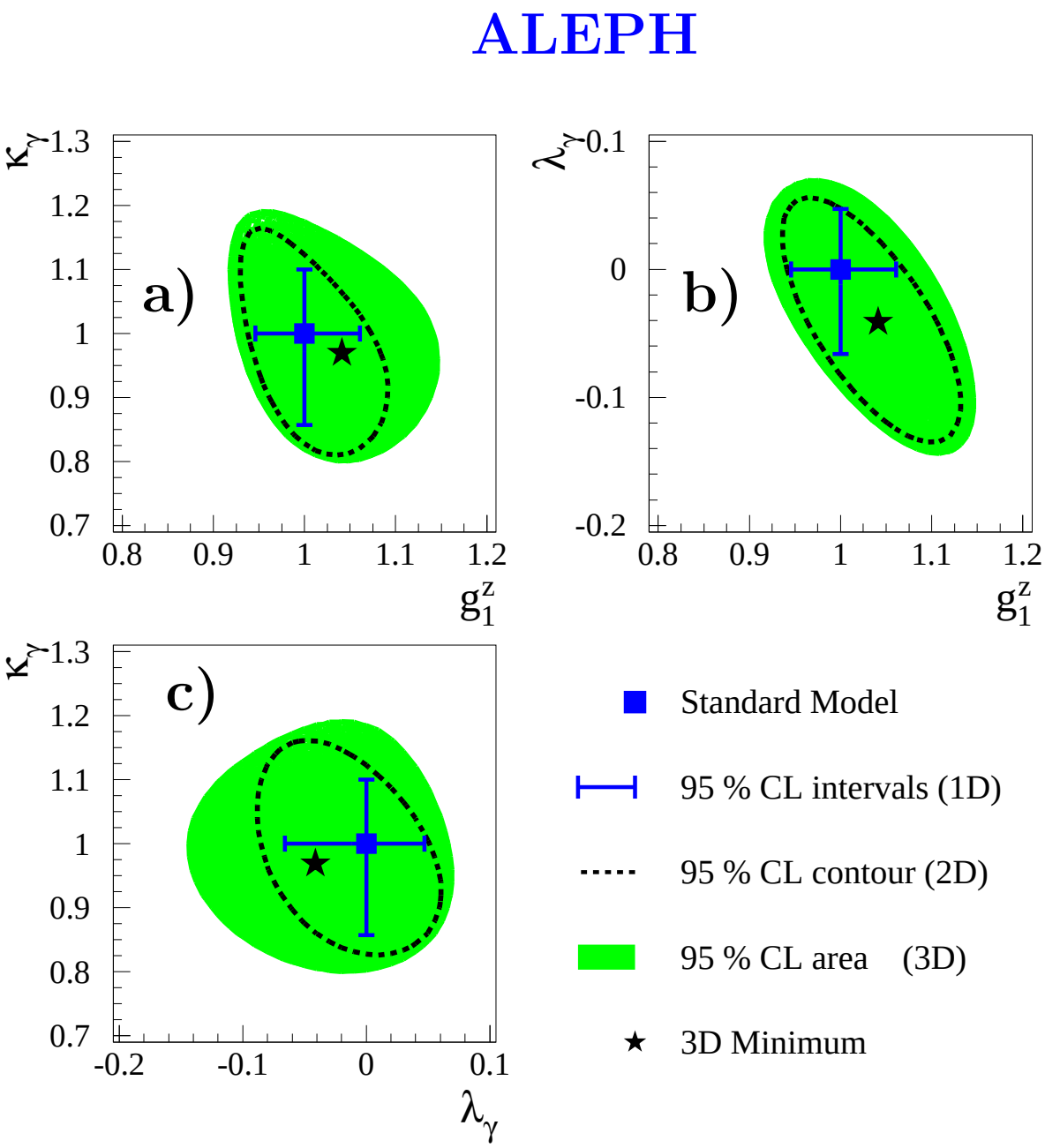

Figure 7: Multi-parameter fits using the combined information from single-γ, single-W and W-pair events including all CM energies. The solid bars indicate the 95 % confidence level (CL) intervals for the single-parameter fit assuming the two others at their Standard Model value. The dashed lines show the 95% confidence level contours of the two-parameter fit. The shaded area is a projection onto the two-dimensional plane of the three-dimensional envelope of the 95% confidence level volume. The most probable value is represented by the star. The Standard Model expectation is represented by a square.